TU/e EINDHOVEN UNIVERSITY OF TECHNOLOGY

Lateral string stability of vehicle platoons

Citation for published version (APA):
Alleleijn, J. H. H. M., Nijmeijer, H., Öncü, S., & Ploeg, J. (2014). *Lateral string stability of vehicle platoons*. (D&C; Vol. 2014.039). Eindhoven University of Technology.

Document status and date:
Published: 01/01/2014

Document Version:
Publisher's PDF, also known as Version of Record (includes final page, issue and volume numbers)

Please check the document version of this publication:

• A submitted manuscript is the version of the article upon submission and before peer-review. There can be important differences between the submitted version and the official published version of record. People interested in the research are advised to contact the author for the final version of the publication, or visit the DOI to the publisher's website.
• The final author version and the galley proof are versions of the publication after peer review.
• The final published version features the final layout of the paper including the volume, issue and page numbers.

Link to publication

General rights
Copyright and moral rights for the publications made accessible in the public portal are retained by the authors and/or other copyright owners and it is a condition of accessing publications that users recognise and abide by the legal requirements associated with these rights.

• Users may download and print one copy of any publication from the public portal for the purpose of private study or research.
• You may not further distribute the material or use it for any profit-making activity or commercial gain
• You may freely distribute the URL identifying the publication in the public portal.

If the publication is distributed under the terms of Article 25fa of the Dutch Copyright Act, indicated by the "Taverne" license above, please follow below link for the End User Agreement:

www.tue.nl/taverne

Take down policy
If you believe that this document breaches copyright please contact us at:

openaccess@tue.nl

providing details and we will investigate your claim.

Download date: 04. Oct. 2023

Lateral string stability of vehicle platoons

J. Alleleijn

DC 2014.039

Master Internship

Coach: dr.ir. S. Öncü (TNO)
dr.ir. J. Ploeg (TNO)

Supervisor: prof.dr. H. Nijmeijer

Eindhoven University of Technology
Department of Mechanical Engineering
Dynamics & Control

TNO
Technical Sciences
Department Integrated Vehicle Safety

Eindhoven, November, 2014

Abstract

This internship report is part of a larger assignment which is an analysis of lateral string stability and the development of a controller design method with guaranteed lateral string stability. Lateral string stability is an issue when a look-ahead sensing method is used in combination with a vehicle-following control strategy. The coupling between vehicles enables errors to increase while they propagate upstream through a string of vehicles. Communicating desired yaw rate or lateral acceleration and use this information for controller design could be an option to achieved guaranteed lateral string stability. One of the applications of lateral control will be conducting maneuvers like merging or lane changes. During these maneuvers the side-slip angles of the tyres stay within the interval of linear tyre response, this means that side-slip angles of the tyres are within $\pm 0.5^{\circ}$. On this interval the non-linear and linearized tyre model have the same linear response. This makes is possible to use a linearized vehicle model with linear tyres for the modeling of the lateral and yaw dynamics of the vehicle. This is validated using experimental data and it is shown that the response of the linearized vehicle model is almost equal to the actual vehicle response.

Contents

Chapter 1

Introduction

In the field of automated driving, a significant amount of research has already been done on longitudinal control of a platoon of vehicles with guaranteed longitudinal string stability. (Shladover et al., 1991; Swaroop, 1997; Shaw and Hedrick, 2007; Naus et al., 2010; Ploeg et al., 2011; Ploeg, 2014). When a platoon is string stabile, errors are attenuated while they propagate upwards through the platoon of vehicles. However, to the author's knowledge there is no controller design method available with guaranteed lateral string stability. This internship report is part of a larger assignment which is an analysis of lateral string stability and the development of a controller design method with guaranteed lateral string stability. The analysis of lateral string stability will be done during the master thesis, while a literature review on lateral control strategies and modeling of the lateral vehicle dynamics will be done during the internship, both assignments will be conducted at TNO in Helmond.

1.1 Background

In a world that becomes more congested every year, the automation of vehicles shows promising results in reducing the congestion. Sinds the 1990's (Shladover et al., 1991) research has been conducted to increase traffic flow by enabling vehicles to drive automated. Already in the 1970's (Peppard, 1974) the observation was made, that when it is possible to attenuate the error propagation along a string of vehicles it would be possible to increase traffic flow. The definition for this is string stability. Extensive research has already been conducted in understanding and developing control methods with guaranteed string stability in longitudinal direction. However, the absence of a controller design method with guaranteed lateral string stability indicates that this areas is not studied sufficiently. Taylor et al. (1999) provide a brief overview about research conducted on lateral control of platoons. Often the methods used for lateral control are highly depending on infrastructure, either via a reference signal embedded in the road, either by lane markers. This dependability on the infrastructure makes the systems expensive and vulnerable to weather influences like snow or mist. Furthermore, situations could occur that vehicles are driving with such small inter-vehicle spacings that it is not possible to detect the lane markings on the road anymore. This makes it necessary to develop a different approach for lateral control.

1.2 Objective

The focus of this internship will be on a literature review on lateral vehicle control strategies, the analysis of lateral vehicle dynamics and validation of the vehicle model currently used by TNO for lateral control application. Furthermore, a non-linear and linearized vehicle model are implemented into the current simulation and different manoeuvres are simulated. Thereafter, simulation results of both models will be compared. Further, experimental data is used to validate whether the vehicle model has a response that is comparable to the actual vehicle response.

1.3 Outline

This report is organized as follows: In Chapter 2, a literature review on lateral control strategies will be presented and in Chapter 3 lateral driving scenarios will analyzed. In Chapter 4, a non-linear and linearized single-track vehicle model will be derived. In Chapter 5 simulations with both models will be performed and the vehicle models will be validated using measurement data. Finally, in Chapter 6 the conclusions and recommendations of the report are presented.

Chapter 2

Literature review

For safe automated driving it is necessary to be able to control both the longitudinal and the lateral movement of a vehicle. Lateral control strategies for vehicle platoons mainly using two sensing methods, look-down sensing or look-ahead sensing. When look-down sensing is considered the sensor(s) look down onto the road surface, while with look-ahead sensing the sensor(s) looks in front of the vehicle. Depending on what sensor(s) is used, they can either be used to detect the road ahead or a vehicle driving in front of the host vehicle. Based on the sensing method, two control strategies are used: lane following or vehicle following. A lane-following control strategy uses sensors to determine where the road ahead is and the lateral position is controlled according to the road. A vehicle-following control strategy uses sensors to determine the relative position of the host vehicle compared to the preceding vehicle and based on this information the lateral position of the vehicle is adapted.

There a several possibilities to what kind of reference frame can be used to determine the position or relative position of a vehicle. Literature can sometimes be ambiguous about the typ of reference frame that is used. Therefore, two reference frames are defined in this literature review, a local and global reference frame. A local reference frame is positioned at the center of gravity of a vehicle oriented according to ISO standards, while all other type of reference frames are called global reference frames. In section 2.1, the objective of this literature review is stated and in Section 2.2 control strategies using look-down sensing are treated. In Section 2.3, control strategies using look ahead sensing are presented, while in Section 2.4 a description of lateral string stability is given and different definitions for lateral string stability found in literature are provided. Finally, Section 2.5 contains the conclusion of this chapter.

2.1 Objective

The aim of this literature study is to provide an overview of the different lateral control strategies and string stability definitions that are currently available in the literature. Papers are first categorized based on the used sensing method, look-down or look-ahead sensing. The second distinction is made based on the used control strategy, lane following or vehicle following.

2.2 Look-down sensing

Look-down sensing is a detection method that was used mainly in the 90's (Shladover et al., 1991; Hingwe and Tomizuka, 1997). This method utilizes a sensor(s) that looks down onto the road surface to detect a reference signal, this reference signal indicates the centerline of the road. This information can be used to calculate the error between the centerline of the road and the position of the vehicle compared to this centerline. This method requires an adaption of the infrastructure, which makes this an expensive method when practically implemented.

2.2.1 Lane following

Lane following is lateral control strategy where a vehicle controls its lateral position accordingly to the curvature of the road. When look-down sensing is used, it is only possible to use a lane following control strategy. Peng and Tomizuka (1990) apply look-down sensing, in combination with a lane-following control strategy. Furthermore, they want to limit the amount of lateral acceleration to maintain a good ride quality by using frequency depending weighting factors. Hingwe and Tomizuka (1997) present an experimental evaluation of a sliding mode controller for lateral vehicle control. Their control objective is to reduce lateral distance error to the road centerline to zero. For the control design they only consider the lateral and yaw dynamics. The center of the road is determined by using magnetic markers embedded in the centerline of the road as a position measurement. Wang and Tomizuka (1999) investigate a robust lane-following approach for a heavy duty vehicle. Their goal is to develop a lane following controller that is robust to model uncertainties. Such as, different road conditions, velocities or different cargo loads for the trailer. The lateral control objective is equal to one in Hingwe and Tomizuka (1997), as well as the use of magnetic markers in the centerline of the road as reference to calculate the lateral error.

2.2.2 Combined longitudinal and lateral vehicle control

Another approach is to combine lateral and longitudinal control of a vehicle, this can be done independently or integrate longitudinal and lateral control into one controller. Lee et al. (1999) choose to independently control the longitudinal and lateral motion of the vehicle. A constant-time headway policy is used for longitudinal control, while a lane-following control strategy is used for lateral control. The platoon in which the vehicles operate is controlled from a centralized position via communication and sends the vehicles in the platoon a reference velocity or acceleration. Rajamani et al. (2000) pursue an approach to integrate lateral and longitudinal movement. In longitudinal direction a constant-time headway policy is utilized, while for lateral control a lane-following control strategy is adopted. Further, Rajamani et al. developed strategies to execute manoeuvres like lane changes and merging, as well as practical integration and validation of the developed strategies and controllers. Kumarawadu and Lee (2006) present a method where a neural network adaptive model-based control algorithm is used, that combines longitudinal and lateral control. The adaptive neural network is used to compensate for modelling errors, non-linearities and coupling effects. The designed controllers minimize the error between the desired longitudinal and lateral position in a global framework.

2.3 Look-ahead sensing

Look-ahead sensing uses a sensor to scan the area in front of the vehicle. In general two types of sensors can be used, a camera or a radar/LIDAR. A radar/LIDAR is only used for vehicle-following control strategies, while a camera can be used for lane following or vehicle following. A camera can detect the lane markings on the road which can be used to determine the centerline of the road. However, it could also be used to detect the preceding vehicle. The largest benefit of look-ahead sensing is that no adaptation of the infrastructure is necessary, this makes it possible to use the control strategies without any extra investment in the current road network.

2.3.1 Lane following

Kosecka et al. (1997) describe an automated steering system based on computer vision, which uses a lane-following control strategy. Furthermore, the influence of the look-ahead distance in relation with the vision processing delay, longitudinal velocity and road geometry is investigated. A vision base approach is developed by Taylor et al. (1999). The vision system estimates the offset from the centre line and the angle between the road tangent and the heading of the vehicle for some look-ahead distance. Furthermore, the vision dynamics are modelled and taken into account into the lateral control law. Taylor et al. investigate what the influence of the vehicle velocity, look-ahead and processing delay is on the performance of the control system in reducing the lateral error. Rossetter and Gerdes (2002) control the lateral movement of the vehicle using a 'virtual' force. This virtual force is regarded as the control input of the vehicle and are viewed as a single force acting upon the vehicle. This force is used to influence the lateral and yaw-dynamics of the vehicle by shifting it along the length of the vehicle. The lateral position of the vehicle is controlled with respect to the centerline of the road and only small deviations of the centerline are considered. Besides the latter, Rossetter and Gerdes use a global reference frame. Both of these design decisions limit the practical application of the developed control algorithm. Rajamani et al. (2003) develop two control strategies based on a non-linear kinematic vehicle model. One is based on the input-state feedback linearization and other controller is based on input-output linearization with stable residual dynamics. The developed control law is set to reduce the tracking error of the x and y axis in a global reference frame. Rajamani et al. experienced that the developed control law worked well in a straight line. However, the control law does not meet their performance criteria on circular road. Therefore, the control law is extended with preview of the road curvature.

2.3.2 Vehicle following

White and Tomizuka (2001) propose to use a laser scanning radar to measure the lateral distance and angle to the preceding vehicle. The angle and lateral position are determined with respect to the frame in the center of gravity of the following vehicle. White and Tomizuka use two trucks for practical implementation. The first truck is manually operated, while the second truck needs to follow the point in the middle at the rear of the first trailer. Furthermore, the movement of the preceding trailer is treated as disturbance and it is assumed that the longitudinal speed and the longitudinal distance are constant. One of the drawbacks of this method is, as stated by the authors, that in the intended highway application, the relative yaw angles can be quite small, making measurement resolution a problem. White and Tomizuka suggest two control objectives, the first one uses the relative lateral position and the second method uses a contour of constant curvature to interpolate a trajectory between the following tractor and preceding vehicle. When the tractor is traveling with a constant yaw and longitudinal velocity the trajectory of the center of gravity of the tractor is approximated by a

circular path. Papadimitriou et al. (2003) propose a lateral vehicle following control problem based on relative lateral distance and angle between two trucks or two passenger vehicles. This approach is suggest to function as back-up in case the lane-following control strategy using look-down sensing fails. The definition of the control objective is depending on whether the considered vehicle is a truck of a passenger car. When a truck with trailer is the considered vehicle, the yaw angle between tractor and trailer is also taken into account. Furthermore, when rear-end tracking is implemented on a tractor-trailer combination serious stability issues are encountered. Papadimitriou et al. managed to overcome these instabilities by increasing the look-ahead distance or reduce the controller gains. However, the first option causes the vehicle to cut corners, while the second solution resultes only in very slow transient behavior. When instead of rear-end tracking, the center of gravity of the preceding vehicle is tracked, a significant reduction of the lateral error is achieved. In Papadimitriou and Tomizuka (2004) this approach is further extended with inter-vehicle communication, for which it is assumed not to have communication delays. The goal of the addition of the communication is to achieve string stable behavior without compromising performance. They incorporate the yaw angle relative to the road frame of the $(i-1)$th vehicle into the control law of the ith vehicle.

A trajectory following control method is developed by Lu and Tomizuka (2003). The trajectory is calculated by using the relative lateral distance between the host and lead vehicle. Further, the effect of different look ahead distances of the LIDAR are investigated. The host vehicle is set to follow the path of the predecessor. The controller is tuned knowing that the road curvature of US highways is limited, this means the area of operation is limited and probably not applicable in Europe due to the smaller corner radii. During testing of the algorithm Lu and Tomizuka (2003) experience lateral stability issues with the developed controller. Lu and Tomizuka improve upon their developed approach from Lu and Tomizuka (2003) in Lu and Tomizuka (2004). Therefore, Lu and Tomizuka equip the vehicles with communication devices. Furthermore, it is stated that when the absolute position of the rear bumper of the preceding vehicle is known the coupling between the two vehicles vanishes, because this information could be used to calculate the global position of the following vehicle. This position of the rear bumper could be measured with GPS or magnetometers, inherently due to the inaccuracy of GPS the system becomes dependent on the infrastructure. The final step in their approach is communicate the lateral error to the centerline of the road to the vehicle behind the host vehicle. A non-linear trajectory generation method in combination with lane following is developed by Awawdeh et al. (2004). The trajectory is generated on-line for all members of the platoon by the platoon leader based on its own movement. The vehicles kinematics are modelled as an object moving in $\mathbb{R}^2$ with a global reference frame. The generated trajectory exactly follows the path of the platoon leader, taken into account the time needed by the platoon member to reach the current position of the platoon leader. The total trajectory for each vehicle is an summation of sub-trajectories which are calculated each variable time step. The size of this time step is depending on the leader's velocity, steering angle and refresh rate of the GPS frequency. However, the inherent inaccuracy of the GPS makes this a difficult and potentially unsafe method to implement. Khatir and Davison (2005) present a decentralized controller with a local reference frame. Furthermore, Khatir and Davison assume that it is possible to measure the distance, angle and velocity to the preceding vehicle, and that the vehicle side-slip angle and angular velocity are known. The vehicle model used for synthesis of the controller includes steering dynamics. The control objective is to minimize the relative angle and minimize the error between the reference and the real inter vehicle space. Khatir and Davison (2006) extend the control strategy developed in Khatir and Davison (2005) with in-line and side tracking. The control objective is to minimize the tracking angle between the centerline of the preceding vehicle and the host vehicle. However, no information is presented on how the required information for the control strategies is obtained. Klančar et al. (2011) developed a control strategy for a differential drive wheeled platoon of mobile robots, using a stereo camera and onboard odometry. A simple kinematic model in combination with a local reference frame is used for a non-

linear controller design. Each robot is able to estimate the trajectory of the preceding vehicle using a second order parametric polynomial and the developed controller is set minimize the error between the actual and desired trajectory.

2.3.3 Combined longitudinal and lateral control

Naffin et al. (2007) independently control the longitudinal and lateral motion of a platoon non-holonomic robots. A decentralized control strategy is used in combination with local sensors. Three different longitudinal control objectives are designed and in lateral direction, minimization of the error between the angle to the preceding robot and the desired angle to that robot is the control objective. Espinosa et al. (2007) introduce a method for designing decentralized overlapping control using a global coordinate system and a linearized kinematic vehicle model. The resulting system is expanded into a higher-dimensional space in which overlapping subsystem appear as disjoint. In this space a fully decentralized control law is designed and the space is contracted again to the original state space. The controllers need to minimize the error between reference and actual x-position and between real and reference y-position of the vehicle. The reference coordinates are provided by the platoon leader and are based on the movement of the platoon leader. Kang et al. (2008) describe a trajectory following method combined with a constant-time headway. A global coordinate frame is used to determine the desired trajectory and a controller is developed that simultaneously reduces longitudinal and lateral error between the desired and actual trajectory. GPS in combination with standard automotive grade Internal Navigation Sensors (INS) are used to determine the position of the vehicle and a GPS base station is used to improve the accuracy of the position measurements. Solyom et al. (2013) present a lateral control method using camera and radar, with the goal to achieve a guaranteed lateral string stable platoon with low cost on-board sensors. Communication is used to achieve longitudinal string stability with small inter-vehicle spacings. Lateral string stability is an important property of a platoon that does not use external references, e.g. road markings. The control objective is to minimize the relative lateral position between two preceding vehicles. The lateral error and control input of the $i-1$ and $i-2$ vehicles are also incorporated in the control input of the ith vehicle and the platoon has to start with zero initial errors. Furthermore, it is assumed the vehicles are driving at a constant longitudinal velocity and the movement of the preceding vehicle is considered as disturbance to the system.

2.4 Lateral stability

The lateral performance of a platoon can be assessed using different methods. One approach is to look at the rearward amplification (RA) of the lateral acceleration. RA quantifies the amount of lateral acceleration magnification of the center of gravity. RA is used in trucks to investigate the stability of truck-trailer combination with one or more trailers. In Luijten (2010) an extensive research has been conducted on the stability of truck-trailer combination with one or more articulations. Furthermore, Luijten provides an overview of the parameters which influence the RA and there effects and concludes further that the amount of yaw dampening decreases when velocity increases. RA can be determined using a time-domain approach (Pauwelussen et al.) or a frequency-domain approach (Fancher and Mathew. (1987)).

Another approach is to use string stability to determine the performance of a string of interconnected systems. When a platoon of vehicles is string stable, occurring errors are attenuated while they propagate along the string of vehicles. Over the years a significant amount of attention is spent

on the development of methods for determining longitudinal string stability of vehicle platoons (Peppard, 1974; Swaroop, 1997; Ploeg et al., 2014). When vehicles are driving in lane-following mode, lateral string stability is less of an issue. All vehicles follow the road and thereby there is no coupling between the vehicles. Due to the absence of coupling a lateral error from one vehicle does not propagate to the next. However, when a vehicle-following control strategy is used lateral string stability becomes an issue. The movement of one vehicle in the platoon directly influences the behavior of the next.

Lateral string stability has received an increase in attention by research over the last couple of years. There are several approaches for determining lateral string stability. Seiler et al. (2003) investigate the stability of bird V-formations. They determine the complementary sensitivity of the lateral error between bird i and bird $i-1$ and the $\mathcal{H}_\infty$ norm of the complementary sensitivity is calculated. Papadimitriou and Tomizuka (2004) are one of the first to validate if their developed approach results into lateral string stable behavior of a platoon of vehicles using the l_∞. The system is string stable in lateral sense when the following definitions holds for non-linear systems:

$$\max_t |y_r^{(i)}(t)| < \max_t |y_r^{(i-1)}(t)| \; \forall \; i \in [2, n],$$

where $y_r^{(i)}$ and $y_r^{(i-1)}$ are the lateral error of the $(i-1)$th and ith vehicle with respect to the road frame, and n is the number of vehicles in the platoon. Khatir and Davison (2005) evaluate the maximum singular values of the transfer function matrices. Solyom et al. (2013) determine l_2 string stability of the lateral error between two preceding vehicles. Due to the two vehicle look-ahead topology, the definition for string stability depends on which vehicle in the platoon is considered. The string stability definition for the first three vehicles is different compared to when $i > 3$.

Another approach is to consider longitudinal and lateral string stability simultaneously, which is known as mesh stability. Pant et al. (2001) investigate mesh stability for a set of point masses for a cluster of unmanned aerial vehicles using the $\mathcal{L}_1$-norm of the impulse response.

2.5 Conclusion

In this literature review two sensing methods and two lateral control strategies are present. When look-down sensing is used the sensor looks straight down onto the road surface, this sensing method was mainly applied in the 90's. The largest drawback of this sensing method is that requires significant investment in the infrastructure and it is also an outdated method. Look-ahead sensing uses sensor(s) that look in front of the vehicle, this method can use either a camera or a radar/LIDAR to look in front of the vehicle. Furthermore, there are two main lateral control strategies, lane following or vehicle following. Lane following can be applied by using look-down sensing or look-ahead sensing. An inductive sensor could be used to detect magnets embedded in the road surface or a camera can be used to detected the lane markings on the road. This information can than be further used to determine the position of the vehicle compared to the centerline of the road. Vehicle following can only be applied when look-ahead sensing is used, this can be achieved either by using a camera or a radar/LIDAR. Furthermore, several approaches for determining lateral stability where presented. One approach is to determine the rearward amplification of the acceleration of the center of mass of the vehicles in the platoon. Another option is determine if a platoon has lateral string-stable behavior. Lateral string stability can be determined by determining l_2-stability for the lateral position error of two preceding vehicle or by calculating the largest singular value of the transfer function. Another possibility is to use the $\mathcal{H}_\infty$-norm for the complementary sensitivity function or the lateral error or combine longitudinal and lateral string stability into mesh-stability and use the $\mathcal{L}_1$-norm of

the impulse response to determine stability. However, to the authors knowledge, there is no literature available about the synthesis of a lateral controller with guaranteed string stability for an infinite string of vehicles.

Chapter 3

Lateral driving manoeuvres

A vehicle can perform different lateral manoeuvres, for example lane changes, merging or talking corners. When driving automated, a vehicle has to be able to perform such manoeuvres. Therefore, a better understanding of the vehicle states is necessary during such a maneuver. This chapter will explain what the type of situations the vehicles will be operating in and provide experimental of such a maneuver is performed. In Section 3.1 the driving scenarios will be explained, in Section 3.2 experimental data of a lane change manoeuvre will be analyzed and Section 3.3 will provide the conclusion of this chapter.

3.1 Driving Scenarios

For the development of automated driving application the main interest at the moment is in three scenarios, lane changes (Figure 3.1a), merging of vehicles (Figure 3.1b) or vehicle following (Figure 3.1c). All scenarios are in a highway type situation, this means that all vehicles drive in the same direction and with longitudinal velocities between 80 and 120km/h. Furthermore, the lane change en merging scenario have high similarities when just the lateral movement of the red vehicle in Figure 3.1a or Figure 3.1b is considered. While during vehicle following on the highway the vehicle states of the following vehicle approximately the same compared to the preceding vehicle. Moreover, when the vehicle is following in the same lane and both vehicles stay in this lane the vehicle states will be even significantly smaller compared to a lane change. Therefore, only experimental data of a lane change scenario will be analyzed.

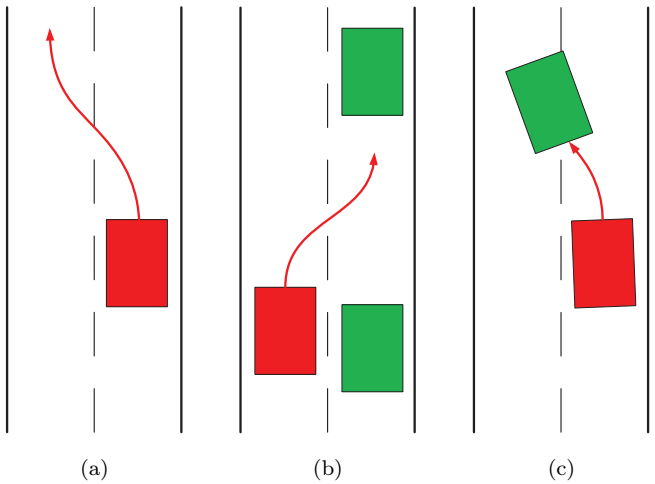

Figure 3.1: (a) A schematic representation of a lane change manoeuver performed bij the red vehicle. (b) A schematic representation of a merging situation executed by the red vehicle. (c) A schematic representation of the vehicle following scenario carried out by the red vehicle.

3.2 Experimental lane-change data

The main interest will be in the steering angles and corresponding yaw rates when a lane change or merging manoeuver is conducted. The special interest in yaw rate is because this is the control input for the low-level steering controller. The experimental data is gathered while driving manually on public highway and performing several fast lane changes. Figure 3.2a and Figure 3.2b contain the longitudinal velocity and steering wheel angle of the test vehicle during the performed lane changes[1].

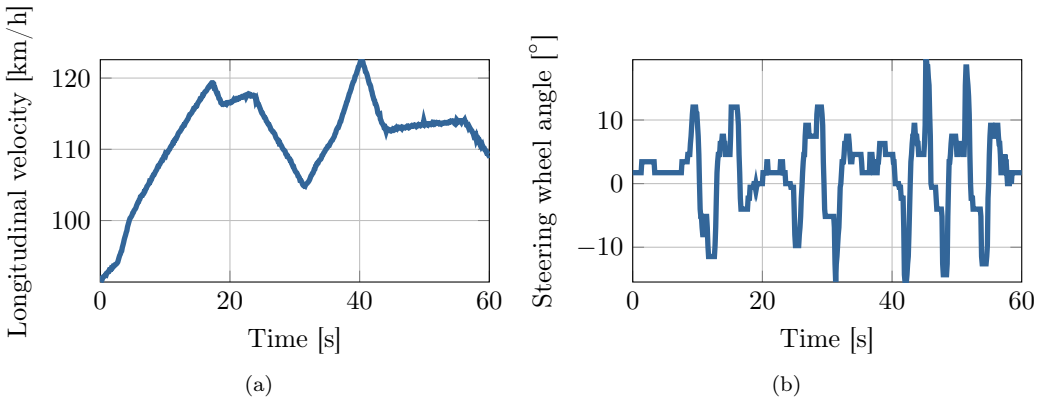

Figure 3.2: (a) Longitudinal velocity of the test vehicle during measurements. (b) Steering wheel angle of the test vehicle during measurements.

[1] Test: `20140430NonSmoothLaneChanging`, file: `log20140430_183427_dat.mat`

The longitudinal velocity of the test vehicle is approximately between 80 and 120km/h. The lane changes are conducted with a quite higher frequency than normally would occur. The high frequency is chosen provide better inside in the minimum and maximum quantities of the yaw rate. Figure 3.3 contains the corresponding yaw rates to the steering angles of Figure 3.2b, as can be seen the maximum yaw rates occurring in these driving conditions is approximately $\pm 5.5 rad/s$.

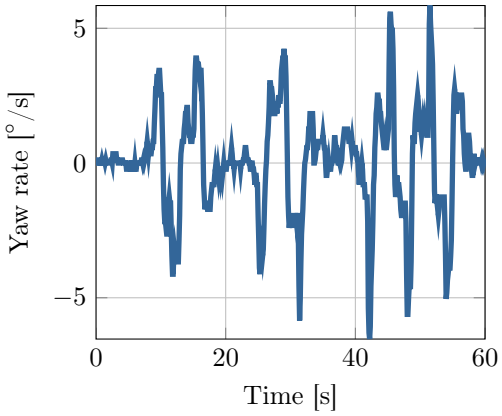

Figure 3.3: The yaw rate of the test vehicle during measurements.

3.3 Conclusion

In this chapter three driving scenarios are presented: lane change, merging and vehicle following. Experimental data is gathered on a lane change manoeuver and the occurring yaw rates of the vehicle are analyzed. The manoeuver is conducted with a high frequency to identify the boundaries of the occurring yaw rate, these boundaries are $\pm 5 rad/s$. The next step is to develop a vehicle model that has representative behavior for manoeuvres like lane changes and vehicle following.

Chapter 4

Lateral vehicle dynamics model

In this chapter a mathematical model of a vehicle is derived, this model will be used for controller design. One of the challenges with modeling is to have a model which has representable behavior without being unnecessary complex. When modeling a vehicle, different approaches can be chosen. One of the possibilities is to model the complete vehicle into a two-track vehicle model. However, this model is elaborate and it is very challenging to use for controller design due to non-linear behavior. Another possibility is to lump the left and right tyres together with the axle characteristics into a single, equivalent "tyre" or axle model. Furthermore, it is assumed that there is no body roll and the model has center-point steering. When a vehicle has center-point steering the tyres are position flat on road, there is no inclination angle or in other words no camber angle. Further, the height of centre of gravity of the vehicle is zero and it is assumed that there is a flat road surface. All these assumptions result into a non-linear single-track vehicle model or bicycle model. In this chapter a non-linear and linearized single-track vehicle model are presented and the equations of motions are derived. Furthermore, the dynamic behaviour of the non-linear and the linearized model are compared to identify under which conditions both models produce the same result. In Section 4.1 the non-linear bicycle model is presented and in Section 4.2 the tyre models are presented. In Section 4.3 the linearized model is derived, Section 4.5 the response of the non-linear and linear tyre models are analyzed and Section 4.6 provides the conclusions of this chapter.

4.1 Non-linear single-track vehicle model

In Figure 4.1, a non-linear single track vehicle model is presented. A single-track vehicle model, is a simplified vehicle where the tyres of the front and the tyre of the rear axle are lumped together into an 'equivalent' tyre. The interest is in the lateral and rotational dynamics of the vehicle. F_{yf}, F_{yr} and F_d are the lateral front tyre force, the lateral rear tyre forces and the drive force acting upon the center of mass (cm) of the vehicle. $\vec{V}_{cm}$, $\vec{V}_f$ and $\vec{V}_r$ are the velocity vectors of the cm of the vehicle and the front and rear tyres, while V_x and V_y are the longitudinal and lateral velocity of the cm in body-fixed frame $\underline{\vec{e}}^1$. $\dot{\psi}_v$ is the rotational velocity of the cm and V_{xf} and V_{yf} are the longitudinal and lateral velocity of the front tyre in frame $\underline{\vec{e}}^2$, while V_{xr} and V_{yr} are the longitudinal and lateral velocity of the rear tyre in frame $\underline{\vec{e}}^1$ Furthermore, α_f, α_r and β are the side-slip angles of front and rear tyres and the side-slip angle of the vehicle, while l_f and l_r are the distances between the cm and the front and rear axle, respectively. $\vec{r}_{f/cm}$ is the vector between the cm and the front tyre, while $\vec{r}_{r/cm}$ is the vector between the cm and the rear tyre.

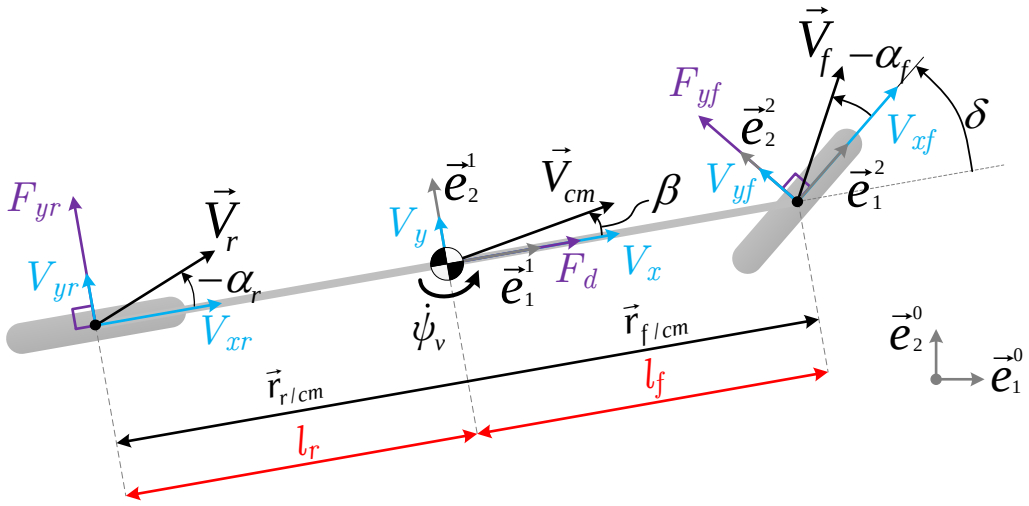

Figure 4.1: Single-track vehicle model

In the derivation of the direction cosine matrices between the different frames $cos(\beta)$ is defined as $C\beta$ and $sin(\beta)$ is defined as $S\beta$. The direction cosine matrix $\underline{A}^{21}$ from frame $\underline{\vec{e}}^{2}$ to frame $\underline{\vec{e}}^{1}$ is defined as:

$$\begin{aligned} \underline{\vec{e}}^{2} &= \underline{A}^{21}\underline{\vec{e}}^{1}, \\ &= \begin{bmatrix} C\delta & S\delta & 0 \\ -S\delta & C\delta & 0 \\ 0 & 0 & 1 \end{bmatrix} \underline{\vec{e}}^{1}. \end{aligned} \tag{4.1}$$

The direction cosine matrix $\underline{A}^{12}$ from frame $\underline{\vec{e}}^{1}$ to frame $\underline{\vec{e}}^{2}$ is defined as:

$$\begin{aligned} \underline{\vec{e}}^{1} &= \underline{A}^{12}\underline{\vec{e}}^{2}, \\ &= \begin{bmatrix} C\delta & -S\delta & 0 \\ S\delta & C\delta & 0 \\ 0 & 0 & 1 \end{bmatrix} \underline{\vec{e}}^{1}. \end{aligned} \tag{4.2}$$

Velocity vector of the center of mass cm of the vehicle is defined as:

$$\begin{aligned} \vec{V}_{cm} &= \underline{V_{cm}}^{1T}\underline{\vec{e}}^{1}, \\ \begin{bmatrix} \dot{x}_v & \dot{y}_v & 0 \end{bmatrix}\underline{\vec{e}}^{1} &= \begin{bmatrix} V_x & V_y & 0 \end{bmatrix}\underline{\vec{e}}^{1}. \end{aligned} \tag{4.3}$$

Acceleration vector of the cm of the vehicle can be derived as follows[1]:

$$\begin{aligned}
\dot{\vec{V}}_{cm} &= \underline{\dot{V}_{cm}}^{1^T}\underline{\vec{e}}^1 + \underline{V_{cm}}^{1^T}\underline{\dot{\vec{e}}}^1, \\
\begin{bmatrix} \ddot{x}_v & \ddot{y}_v & 0 \end{bmatrix}\underline{\vec{e}}^1 &= \underline{\dot{V}_{cm}}^{1^T} - \underline{V_{cm}}^{1^T}{}^1\underline{\tilde{\omega}}\,\underline{\vec{e}}^1, \\
&= \begin{bmatrix} \dot{V}_x & \dot{V}_y & 0 \end{bmatrix}\underline{\vec{e}}^1 - \begin{bmatrix} V_x & V_y & 0 \end{bmatrix}\begin{bmatrix} 0 & -\dot{\psi}_v & 0 \\ \dot{\psi}_v & 0 & 0 \\ 0 & 0 & 0 \end{bmatrix}\underline{\vec{e}}^1, \\
&= \begin{bmatrix} \dot{V}_x & \dot{V}_y & 0 \end{bmatrix}^T\underline{\vec{e}}^1 - \begin{bmatrix} V_y\dot{\psi}_v & -V_x\dot{\psi}_v & 0 \end{bmatrix}^T\underline{\vec{e}}^1, \\
&= \begin{bmatrix} \dot{V}_x - V_y\dot{\psi}_v & \dot{V}_y + V_x\dot{\psi}_v & 0 \end{bmatrix}^T\underline{\vec{e}}^1. \qquad (4.4)
\end{aligned}$$

Translational equation of motion of the cm:

$$\begin{aligned}
m\dot{\vec{V}}_{cm} &= \sum \vec{F} = \vec{F}_{yf} + \vec{F}_{yr} + \vec{F}_d, \\
m\underline{\dot{V}_{cm}}^{1^T}\underline{\vec{e}}^1 &= \underline{F_f}^{2^T}\underline{A}^{21}\underline{\vec{e}}^1 + \underline{F_r}^{1^T}\underline{\vec{e}}^1 + \underline{F_d}^{1^T}\underline{\vec{e}}^1, \\
m\begin{bmatrix} \ddot{x}_v \\ \ddot{y}_v \\ 0 \end{bmatrix}^T\underline{\vec{e}}^1 &= \begin{bmatrix} 0 \\ F_{yf} \\ 0 \end{bmatrix}^T\begin{bmatrix} C\delta & S\delta & 0 \\ -S\delta & C\delta & 0 \\ 0 & 0 & 1 \end{bmatrix}\underline{\vec{e}}^1 + \begin{bmatrix} 0 \\ F_{yr} \\ 0 \end{bmatrix}^T\underline{\vec{e}}^1 + \begin{bmatrix} F_d \\ 0 \\ 0 \end{bmatrix}^T\underline{\vec{e}}^1, \\
&= \begin{bmatrix} -F_{yf}S\delta + F_d \\ F_{yf}C\delta + F_{yr} \\ 0 \end{bmatrix}^T\underline{\vec{e}}^1. \qquad (4.5)
\end{aligned}$$

Rotational equation of motion of the vehicle (the rotation is only around $\vec{e}_3^1$):

$$\begin{aligned}
\sum \vec{M} &= \mathbf{J}\cdot\dot{\vec{\omega}} + \vec{\omega}\times(\mathbf{J}\cdot\vec{\omega}), \\
\begin{bmatrix} \sum M_x & \sum M_y & \sum M_z \end{bmatrix}^T\underline{\vec{e}}^1 &= I_z\underline{\vec{e}}_3^1\underline{\vec{e}}_3^1\cdot\ddot{\psi}_v + \dot{\psi}_v\underline{\vec{e}}_3^1\times\left(I_z\underline{\vec{e}}_3^1\underline{\vec{e}}_3^1\cdot\dot{\psi}_v\underline{\vec{e}}_3^1\right), \\
\begin{bmatrix} 0 & 0 & \sum M_z \end{bmatrix}^T\underline{\vec{e}}^1 &= \begin{bmatrix} 0 & 0 & I_z\ddot{\psi}_v \end{bmatrix}^T\underline{\vec{e}}^1, \\
\sum M_z\underline{\vec{e}}_3^1 &= I_z\ddot{\psi}_v\underline{\vec{e}}_3^1. \qquad (4.6)
\end{aligned}$$

$$\begin{aligned}
M_z\underline{\vec{e}}_3^1 &= \vec{r}_{f/cm}\times\vec{F}_{yf} + \vec{r}_{r/cm}\times\vec{F}_{yr}, \\
&= \begin{bmatrix} l_f \\ 0 \\ 0 \end{bmatrix}^T\underline{\vec{e}}^1\times\begin{bmatrix} -F_{yf}S\delta \\ F_{yf}C\delta \\ 0 \end{bmatrix}^T\underline{\vec{e}}^1 + \begin{bmatrix} -l_r \\ 0 \\ 0 \end{bmatrix}^T\underline{\vec{e}}^1\times\begin{bmatrix} 0 \\ F_{yr} \\ 0 \end{bmatrix}^T\underline{\vec{e}}^1, \\
&= \begin{bmatrix} 0 & 0 & l_fF_{yf}C\delta \end{bmatrix}\underline{\vec{e}}^1 + \begin{bmatrix} 0 & 0 & -l_rF_r \end{bmatrix}\underline{\vec{e}}^1, \\
&= (l_fF_{yf}C\delta - l_rF_{yr})\,\underline{\vec{e}}_3^1. \qquad (4.7)
\end{aligned}$$

When (4.7) is substituted in (4.6), the equation is obtained for the rotational dynamics of the vehicle:

$$(l_fF_{yf}C\delta - l_rF_{yr}) = I_z\ddot{\psi}_v. \qquad (4.8)$$

[1] $\underline{\dot{\vec{e}}}^1$, is calculated using the Poisson equation presented in van de Wouw (2010), Appendix B

Equations of motion around the cm of the vehicle are:

$$\begin{aligned}\begin{bmatrix} \sum F_x \\ \sum F_y \\ \sum M_z \end{bmatrix}^T \underline{\vec{e}}^1 &= \begin{bmatrix} m\ddot{x}_v \\ m\ddot{y}_v \\ I_z\ddot{\psi}_v \end{bmatrix}^T \underline{\vec{e}}^1, \\ &= \begin{bmatrix} m\left(\dot{V}_x - V_y\dot{\psi}_v\right) \\ m\left(\dot{V}_y + V_x\dot{\psi}_v\right) \\ I_z\ddot{\psi}_v \end{bmatrix}^T \underline{\vec{e}}^1. \end{aligned} \tag{4.9}$$

When (4.5) and (4.8) is substituted in (4.9), the translation and rotation of the cm of the vehicle in frame $\underline{\vec{e}}^1$ can be described as follows:

$$\begin{bmatrix} m\left(\dot{V}_x - V_y\dot{\psi}_v\right) \\ m\left(\dot{V}_y + V_x\dot{\psi}_v\right) \\ I_z\ddot{\psi}_v \end{bmatrix}^T \underline{\vec{e}}^1 = \begin{bmatrix} -F_{yf}S\delta + F_d \\ F_{yf}C\delta + F_{yr} \\ l_f F_{yf}C\delta - l_r F_{yr} \end{bmatrix}^T \underline{\vec{e}}^1. \tag{4.10}$$

The lateral force at the front and rear tyre, F_{yf} and F_{yr}, are depending on the side-slip angle α_f and α_r of the front and rear tyre, respectively.

4.2 Tyre models

There are two main approaches for the modeling of the tyre. One uses a non-linear tyre model, while another approach is to use a linearized tyre model.

4.2.1 Non-linear tyre model

An example of a non-linear tyre model is the Magic Formula developed by Pacejka (2005). The Magic Formula is non-linear mathematical model that describes tyre behaviour based on empirical data. The tyre characteristics of the test vehicle used by TNO has been measured and a tyre model has been derived using the Tyre estimator[2] and Magic Formula. Figure 4.2a contains an example of the lateral tyre forces as function of the side-slip angle. The side-slip angle (α) is calculated by taking the arctangent of the lateral velocity (V_{yi}) and the longitudinal velocity (V_{xi}) of the tyre, where i indicates the front or rear tyre, respectively:

$$\alpha = atan\left(\frac{V_{yi}}{V_{xi}}\right), \quad i \in \{f, r\}. \tag{4.11}$$

[2] https://www.tno.nl/content.cfm?context=thema&content=prop_case&laag1=894&laag2=914&laag3=104&item_id=1790&Taal=2

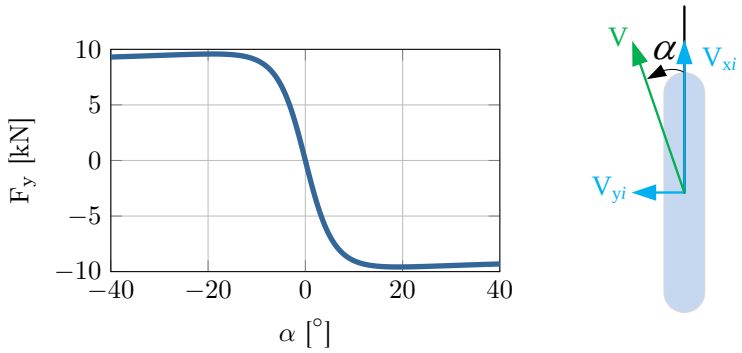

(a) (b)

Figure 4.2: (a) An example of a non-linear tyre characteristic produced by the Magic Formula. (b) Calculation of the side-slip angle of the tyre (α), V is the velocity vector of the tyre, V_{xi} and V_{yi} are the longitudinal and lateral velocity of the front or rear tyre, respectively.

The velocity of the front tyre can be calculated as follows:

$$
\begin{aligned}
\vec{V}_f &= \vec{V}_{cm} + \dot{\vec{r}}_{f/cm}, \\
\begin{bmatrix} V_{xf} & V_{yf} & 0 \end{bmatrix} \underline{\vec{e}}^2 &= \underline{V}_{cm}{}^{1T} \underline{A}^{12} \underline{\vec{e}}^2 - \underline{r}_{f/cm}{}^{1T} {}^{10}\underline{\tilde{\omega}}^1 \underline{A}^{12} \underline{\vec{e}}^2, \\
&= \begin{bmatrix} V_x & V_y & 0 \end{bmatrix} \begin{bmatrix} C\delta & -S\delta & 0 \\ S\delta & C\delta & 0 \\ 0 & 0 & 1 \end{bmatrix} \underline{\vec{e}}^2 \\
&\quad - \begin{bmatrix} l_f \\ 0 \\ 0 \end{bmatrix}^T \begin{bmatrix} 0 & -\dot{\psi}_v & 0 \\ \dot{\psi}_v & 0 & 0 \\ 0 & 0 & 0 \end{bmatrix} \begin{bmatrix} C\delta & -S\delta & 0 \\ S\delta & C\delta & 0 \\ 0 & 0 & 1 \end{bmatrix} \underline{\vec{e}}^2, \\
&= \begin{bmatrix} V_x C\delta + V_y S\delta \\ -V_x S\delta + V_y C\delta \\ 0 \end{bmatrix}^T \underline{\vec{e}}^2 - \begin{bmatrix} -l_f S\delta \dot{\psi}_v \\ -l_f C\delta \dot{\psi}_v \\ 0 \end{bmatrix} \underline{\vec{e}}^2, \\
&= \begin{bmatrix} V_x C\delta + \left(V_y + l_f \dot{\psi}_v\right) S\delta \\ -V_x S\delta + \left(V_y + l_f \dot{\psi}_v\right) C\delta \\ 0 \end{bmatrix} \underline{\vec{e}}^2.
\end{aligned} \tag{4.12}
$$

Velocity rear tyre is derived as follows:

$$
\begin{aligned}
\vec{V}_r &= \vec{V}_{cm} + \dot{\vec{r}}_{r/cm}, \\
\begin{bmatrix} V_{xr} & V_{yr} & 0 \end{bmatrix} \underline{\vec{e}}^1 &= \underline{V}_{cm}{}^{1T} \underline{\vec{e}}^1 - \underline{r}_{r/cm}{}^{1T} {}^{10}\underline{\tilde{\omega}}^1 \underline{\vec{e}}^1, \\
&= \begin{bmatrix} V_x \\ V_y \\ 0 \end{bmatrix}^T \underline{\vec{e}}^1 - \begin{bmatrix} -l_r \\ 0 \\ 0 \end{bmatrix}^T \begin{bmatrix} 0 & -\dot{\psi}_v & 0 \\ \dot{\psi}_v & 0 & 0 \\ 0 & 0 & 0 \end{bmatrix} \underline{\vec{e}}^1, \\
&= \begin{bmatrix} V_x & V_y - l_r \dot{\psi}_v & 0 \end{bmatrix} \underline{\vec{e}}^1.
\end{aligned} \tag{4.13}
$$

4.2.2 Linear tyre model

The non-linear Magic Formula can also be linearized and reduced to a multiplication between the side-slip angle (α) and the lateral tyre stiffness (C_i) (4.14). However, linearizing the tyre model also imposes limitations on the size of the side-slip angles for which the model still is representative for the actual developed lateral tyre forces.

$$F_{yi} = -C_i \alpha_i, \tag{4.14}$$

where i is the front or rear tyre, C_i is the lateral stiffness of the tyre and α is the side-slip angle of the tyre. The linearized tyre model is only valid when the side-slip angles stay within $\pm 0.5°$. When equation (4.11), (4.12) and (4.13) are substituted in (4.14) the following equations for the front and rear tyre forces are obtained:

$$F_{yf} = -C_f atan\left(\frac{-V_x S\delta + \left(V_y + l_f\dot{\psi}_v\right) C\delta}{V_x C\delta + \left(V_y + l_f\dot{\psi}_v\right) S\delta}\right), \tag{4.15}$$

$$F_{yr} = -C_r atan\left(\frac{V_y - l_r\dot{\psi}_v}{V_x}\right). \tag{4.16}$$

4.3 Linearized single-track vehicle model

One of the drawbacks of the non-linear model is that linear control theory and linear stability analysis is not applicable anymore. When it is assumed that the driving force F_d in equation (4.10) is available such that $\dot{V}_x = 0$, the following vehicle dynamic model is obtained, which describes the lateral and rotational dynamics of the cm of the vehicle, where V_y and $\ddot{\psi}_v$ are chosen as generalized coordinates. This model is also presented in Pacejka (2005) and Rajamani (2011).

$$\begin{bmatrix} \dot{V}_y \\ \ddot{\psi}_v \end{bmatrix}^T \underline{\vec{e}}^1 = \begin{bmatrix} \frac{-1}{m}\left(F_{yf} C\delta + F_{yr}\right) - V_x\dot{\psi}_v \\ \frac{-1}{I_z}\left(l_f F_{yf} C\delta - l_r F_{yr}\right) \end{bmatrix}^T \underline{\vec{e}}^1. \tag{4.17}$$

Equation (4.15) and (4.16) can be substituted in (4.17) resulting in:

$$\begin{bmatrix} \dot{V}_y \\ \ddot{\psi}_v \end{bmatrix}^T \underline{\vec{e}}^1 = \begin{bmatrix} \frac{-1}{m}\left(C\delta C_f atan\left(\frac{-V_x S\delta + \left(V_y + l_f\dot{\psi}_v\right) C\delta}{V_x C\delta + \left(V_y + l_f\dot{\psi}_v\right) S\delta}\right) + C_r atan\left(\frac{V_y - l_r\dot{\psi}_v}{V_x}\right)\right) - V_x\dot{\psi}_v \\ \frac{-1}{I_z}\left(l_f C\delta C_f atan\left(\frac{-V_x S\delta + \left(V_y + l_f\dot{\psi}_v\right) C\delta}{V_x C\delta + \left(V_y + l_f\dot{\psi}_v\right) S\delta}\right) - l_r C_r atan\left(\frac{V_y - l_r\dot{\psi}_v}{V_x}\right)\right) \end{bmatrix}^T \underline{\vec{e}}^1. \tag{4.18}$$

When the it is assumed that all angles are small ($\delta < 10°$, $atan(\alpha) = \alpha$) and that V_x is constant, equation (4.18) can be linearized, resulting into:

$$\begin{bmatrix} \dot{V}_y \\ \ddot{\psi}_v \end{bmatrix}^T \underline{\vec{e}}^1 = \begin{bmatrix} \frac{-1}{m}\left(C_f\left(\frac{-V_x\delta + \left(V_y + l_f\dot{\psi}_v\right)}{V_x + \left(V_y + l_f\dot{\psi}_v\right)\delta}\right) + C_r\left(\frac{V_y - l_r\dot{\psi}_v}{V_x}\right)\right) - V_x\dot{\psi}_v \\ \frac{-1}{I_z}\left(l_f C_f\left(\frac{-V_x\delta + \left(V_y + l_f\dot{\psi}_v\right)}{V_x + \left(V_y + l_f\dot{\psi}_v\right)\delta}\right) - l_r C_r\left(\frac{V_y - l_r\dot{\psi}_v}{V_x}\right)\right) \end{bmatrix}^T \underline{\vec{e}}^1 \tag{4.19}$$

Under the assumption that the vehicle is driving in a steady state, with constant velocity on a straight road or a road with large corner radii, term $\left(V_y + l_f\dot{\psi}_v\right)\delta$ can be neglected, due to its small contribution compared to the longitudinal velocity V_x. This results in the following linearized-differential equations for the lateral and rotational dynamics:

$$\begin{bmatrix} \dot{V}_y \\ \ddot{\psi}_v \end{bmatrix}^T \underline{\vec{e}}^1 = \begin{bmatrix} \frac{C_f}{m}\left(\delta - \frac{V_y+\dot{\psi}_v l_f}{V_x}\right) - \frac{C_r}{m}\left(\frac{V_y-\dot{\psi}_v l_r}{V_x}\right) - V_x\dot{\psi}_v \\ \frac{C_f l_f}{I_z}\left(\delta - \frac{V_y+\dot{\psi}_v l_f}{V_x}\right) + \frac{C_r l_r}{I_z}\left(\frac{V_y-\dot{\psi}_v l_r}{V_x}\right) \end{bmatrix}^T \underline{\vec{e}}^1 \tag{4.20}$$

4.4 Linearized vehicle model in state-space form

Equation (4.20) can be written in state space form with $x = \begin{bmatrix} V_y & \dot{\psi}_v \end{bmatrix}^T$ and δ chosen as input, resulting in:

$$\begin{aligned} \dot{x} &= Ax + Bu \\ \begin{bmatrix} \dot{V}_y \\ \ddot{\psi}_v \end{bmatrix} &= \begin{bmatrix} -\frac{C_f+C_r}{mV_x} & -\left(\frac{C_f l_f - C_r l_r}{mV_x} + V_x\right) \\ -\frac{C_f l_f - C_r l_r}{I_z V_x} & -\frac{C_f l_f^2 + C_r l_r^2}{I_z V_x} \end{bmatrix} \begin{bmatrix} V_y \\ \dot{\psi}_v \end{bmatrix} + \begin{bmatrix} \frac{C_f}{m} \\ \frac{C_f l_f}{I_z} \end{bmatrix} \delta \end{aligned} \tag{4.21}$$

4.5 Interval linear tyre response

As stated in subsection 4.2.2 the non-linear and linearized tyre model have a small interval on which both tyre models have the same response. In Figure 4.3a and 4.3b the front and rear tyre characteristics of the non-linear and linear tyre model are presented.

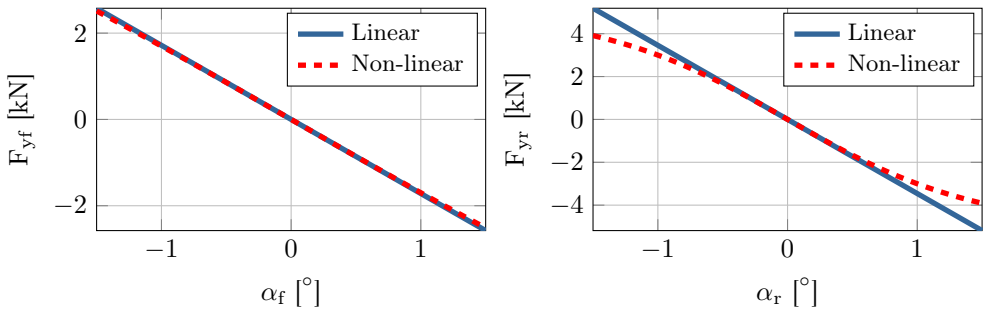

(a) (b)

Figure 4.3: (a) Lateral forces as function of the slip angles of the non-linear and linear tyre model for the front axle. (b) Lateral forces as function of the slip angles of the non-linear and linear tyre model for the rear axle.

As can be observed, both tyre models develop almost same lateral forces when the side-slip angle of the tyres stay within the interval of $-0.5° < \alpha < 0.5°$. This means that the results of the linearized

vehicle model with linear tyres are only valid when the tyre side-slip angles are within $\pm 0.5°$. If the side-slip angles are outside of this interval, the lateral forces calculated by the linearized model will be larger than actually possible. The simplifications of the linearized model cause an significant increase in the inaccuracy of the model when the side-slip angles become larger then interval on which the tyres have a linear response. On the interval of $-0.5° < \alpha < 0.5°$, the Root Mean Square Error (RMSE) between the non-linear and linearized model for the front tyre is $0.52N$ and for the rear tyre $23.9N$. Although the RMSE of the rear tyre model is larger, it is still acceptable. The largest errors occur at $-0.5°$ or $0.5°$, at these slip angles the relative error are only 0.06% for the front tyre and 1.44% for the rear tyre. Furthermore, the RMSE for the front tyre on interval $-1° < \alpha < 1°$ is only $6.85N$, which is 0.39%.

4.6 Conclusion

In this chapter a non-linear vehicle model with non-linear tyre models and a linearized vehicle model with linear tyre models is presented. For both models the equations of motion for the lateral and yaw dynamics are derived. The non-linear model provides an accurate representation of the actual vehicle response. However, this model prevents the application of linear control theory and linear stability analysis. On the other hand, the linearized model is not always representative for the actual vehicle behavior, this especially occurs with large side-slip angles of the tyres. Therefore, an analysis is performed to identify under which conditions the linearized and non-linear tyre model have the same response. It is shown that when the side-slip angles of the tyres stay within $\pm 0.5°$, both tyre models develop almost same lateral forces. The next step will be to investigate if the vehicle response of both the non-linear and linearized model is also the same when the side-slip angles stay within $\pm 0.5°$.

Chapter 5

Simulations of the vehicle dynamics model

In Chapter 4 a non-linear vehicle model with non-linear tyre models and a linearized vehicle model with linearized tyre models is presented. It is shown that when the side slip angle of the tyres stay within $\pm 0.5^{\circ}$ the tyres response of the non-linear and linearized model are almost equal. This means that the linearized tyre provides a response which represents the actual tyre response within this interval. In this chapter, the dynamic behavior of the non-linear and linearized vehicle model developed in chapter 4 is further analyzed. The goal of this analysis is to investigate if the dynamic response of the vehicle models are also almost equal when staying within the interval of linear the tyre response. Special attention will be given to the dynamic response of both models when the same steer input is provided, while insuring the side-slip angles of the tyres do not exceed $\pm 0.5^{\circ}$. In Section 5.1 a sinus steer will be simulated and the results are presented and analyzed, in Section 5.2 the CACC simulation model of TNO will be used to simulate a lane change and results are analyzed. In Section 5.3 the non-linear and linearized models are compared to real experimental data and finally, Section 5.4 contains the conclusion of this chapter.

5.1 Simulation vehicle models

Table 5.1 provides the values used for the vehicle parameters in the simulation model. These values are obtained by conducting measurements on one of the Toyota Prius used by TNO for CACC development.

Mass (front + rear) axle $[kg]$	958 + 667
Moment of inertia $[kgm^2]$	2865.61
Wheel base $[m]$	2.7
Distance COG to front axle $[m]$	1.1082
Distance COG to rear axle $[m]$	1.5918
Steering house ratio [-]	15.6483
Lateral stiffness front tyre $[\frac{N}{rad}]$	98389
Lateral stiffness rear tyre $[\frac{N}{rad}]$	198142
Tire radius [m]	0.31265

Table 5.1: Vehicle parameters used for simulation.

The first simulation is performed with a constant longitudinal velocity of $80km/h$. A sinusoidal steering angle input is used, Figure 5.1 presents the steering angles of the front wheels (δ_{wheel}). A sinusoidal steering input is chosen because, this signal represents continues lane changes performed by a vehicle. Furthermore, it provides the possibility to investigate possible different dynamic behavior of the vehicle to positive of negative side-slip angles.

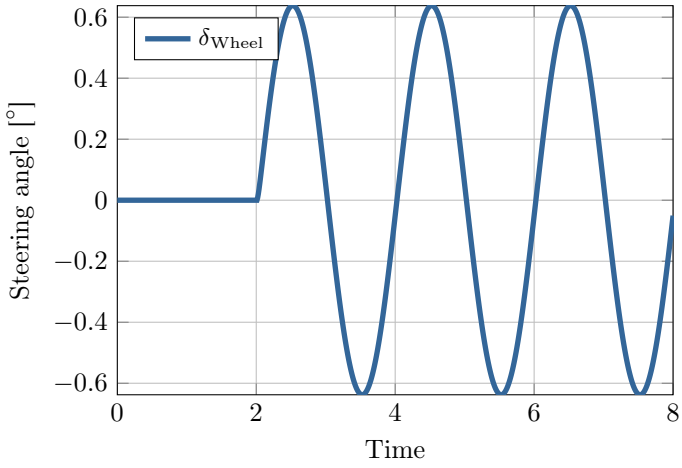

Figure 5.1: Steering angle reference signal used during the simulation.

First, the side-slip angles of the front and rear tyres are compared. As can be seen in Figure 5.2a and Figure 5.2b, the side-slip angles achieved by the non-linear and linearized model appear to be the same for the front and rear tyres. Furthermore, the side-slip angles stay within in the interval of $\pm 0.5°$. The Root Mean Square Error (RMSE) between the non-linear and linearized model for the front tyre and rear tyre is $0.00026N$, which is a relative error of 0.05%.

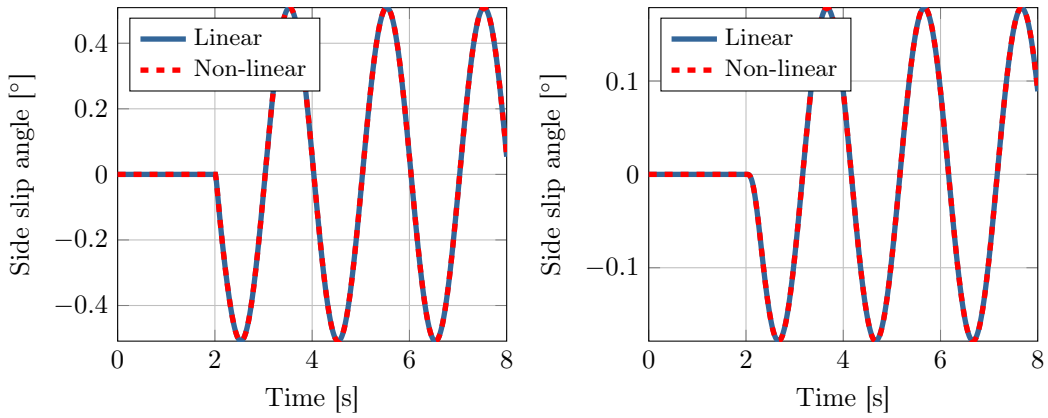

(a) (b)

Figure 5.2: (a) Side-slip angles of the front tyre of the non-linear and linearized model. (b) Side-slip angles of the rear tyre of the non-linear and linearized model.

Similar results can be observed when the lateral acceleration (Figure 5.3a) and vehicle side-slip angle are considered (Figure 5.3b). The RMSE for the lateral acceleration is $0.00064 m/s^2$ or 0.07%, and for the vehicle side-slip angle the RMSE is $0.00025°$ or 0.6%.

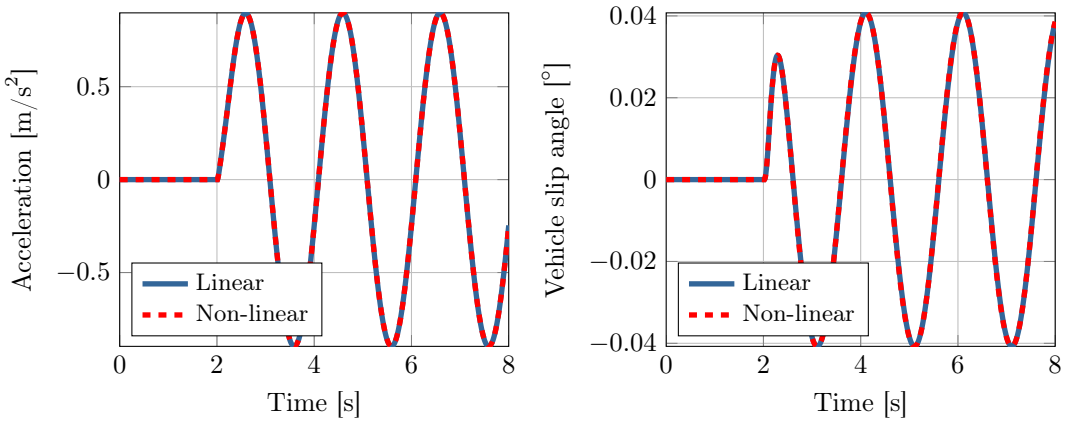

(a) (b)

Figure 5.3: (a) Lateral acceleration of the non-linear and linearized vehicle models. (b) Vehicle side-slip angle of the non-linear and linearized model.

Figure 5.4 presents the yaw-rate responses of both models. The RMSE between both models is $0.00074 \circ/s$ or 0.03%. The yaw rates are lower than measured in Section 3.2. Furthermore, the side-slip angles of the front tyres (Figure 5.2a) are already at the maximum allowed $\pm 0.5°$. These are the upper and lower boundaries for the slide-slip angles for which the tyres have guaranteed linear behavior. This means that the maneuvers performed in Section 3.2 are already causing, to some

extent, non-linear behavior in the tyres. The non-linear and linearized model will produce different results if this experimental data will be used for validation of the models.

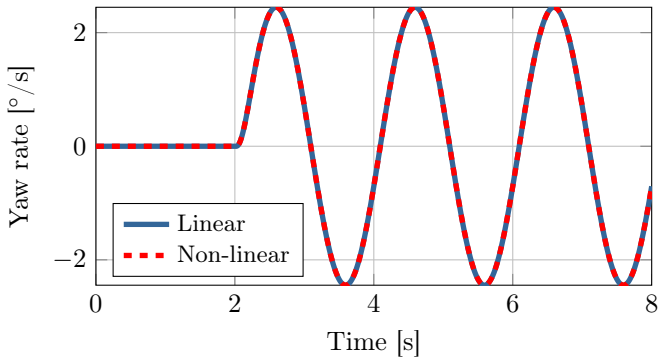

Figure 5.4: The yaw-rate response of the non-linear and linearized vehicle model.

5.2 Simulation model TNO

The next step is to implement both vehicle models in the Simulink model of TNO. This Simulink model is used for the development of any number of cooperative driving applications, the model can consist of any number of vehicles with different sensors and devices necessary for cooperative driving. Each vehicle model consists of a user, Wi-Fi communication, radar, camera, GPS, several other sensors which measure the state of the vehicle, a real-time controller and a vehicle model. The controllers will be used as they are present in the model without going into further details about the kind of controllers or used control strategies.

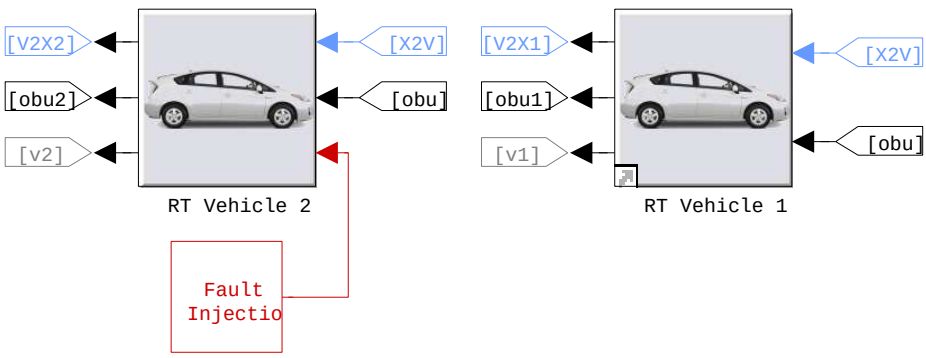

Figure 5.5: Simulink model used by TNO for the simulation of cooperative driving applications.

The focus of the simulations will be to investigate the response of the non-linear and linearized

vehicle models. The actuation of the electric motor of the steering mechanism of the vehicle is conducted by a separate controller, also know as a low-level steering controller. This low-level controller receives information from the vehicle model which is used to calculate the necessary control input. The low-level controller uses the desired yaw-rate of the vehicle as input. Therefore, the focus of the simulations will be on the yaw-rate response of both the non-linear and the linearized vehicle models.

5.2.1 Lane change simulation

One of the manoeuvres an automated driving vehicle has to be able to perform is a lane change at high velocity. The simulation is conducted at a constant longitudinal velocity of $80km/h$ and the signal in Figure 5.6 is used as a reference signal for the steering angle.

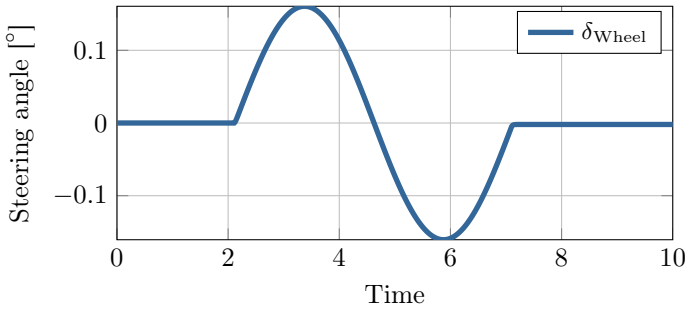

Figure 5.6: Steer input used to induce a lane change manoeuver.

Figure 5.7 contains the yaw-rate response of both vehicle models to this steering input. The RMSE between the models is $0.0001°/s$ or 0.016%.

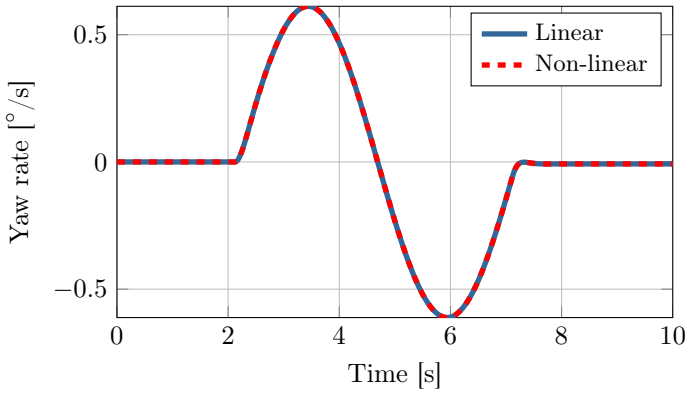

Figure 5.7: Yaw-rate response of the non-linear and linearized vehicle models to the steering input presented in Figure 5.6.

5.2.2 Model limitations

The space model derived in Chapter 4 is a Linear Parametric Varying (LPV) model, with the longitudinal velocity V_x as the varying parameter. When this parameter is changed, the eigenvalues of state space model change and thereby the time response of the model to an input signal changes. An eigenvalue analysis of the linearized model shows that both eigenvalues are in the LHP when $V_x > 0m/s$. This means that the model should be stable for all $V_x > 0m/s$. However, when a simulation is performed with a velocity of $0.9m/s$, the model becomes unstable (Figure 5.8). The steering input remains to equal to the one in Figure 5.6.

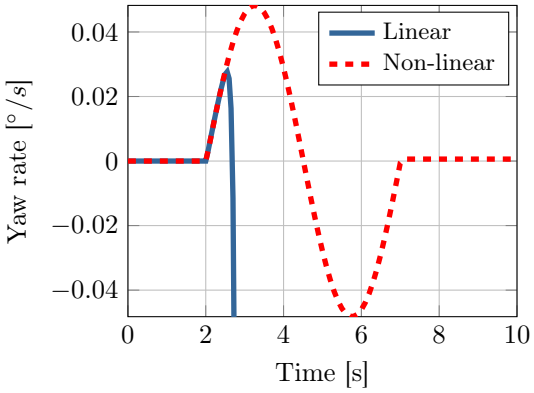

Figure 5.8: Yaw-rate response of the stable non-linear and unstable linearized vehicle model.

This instability is due to the use of an numerical solver. When the velocity of the vehicle model is lowered, the eigenvalues of the model (4.21) increase. The time-response of the system can be calculate using:

$$y(t) = Ce^{At}x_0, \tag{5.1}$$

where C is the output matrix, which assumed to be equal to the identity matrix. A is the system matrix and x_0 are the initial conditions. Matrix A is diagonalizable and therefore (5.1) can be rewritten into:

$$y(t) = Me^{Jt}M^{-1}x_0, \tag{5.2}$$

Where M is the singularity transformation matrix, and matrix J is the Jordan form, which is equal to:

$$J = \begin{bmatrix} \lambda_1 & 0 \\ 0 & \lambda_2 \end{bmatrix} \tag{5.3}$$

The simulation has a sample frequency of $100Hz$, when one or both of the eigenvalues are larger than the half sample frequency used in the model, the corresponding dynamical response of the model becomes faster than that is sampled. This causes an instability in the model. One solution could be to increase the sample frequency. However, this would only postpone the stability issues of the simulation model. A better solution would be to use a kinematic model at low velocities, at low velocities there is almost no dynamic behavior of the tyres anymore and a kinematic would have the same dynamical response as the non-linear or linearized, without causing numerical problems. The velocity corresponding with an eigenvalue equal to $2\pi 50$, is $0.944m/s$.

5.3 Experimental data

The final step is to validate if the response of the simulation models are representable for the actual vehicle response. Therefore, experimental data was gathered at the ATC test track in Aldenhoven on the 8th of May 2014[1]. Figure 5.9a presents the sinusoidal steer angle, while Figure 5.9b contains the velocity signal of the vehicle.

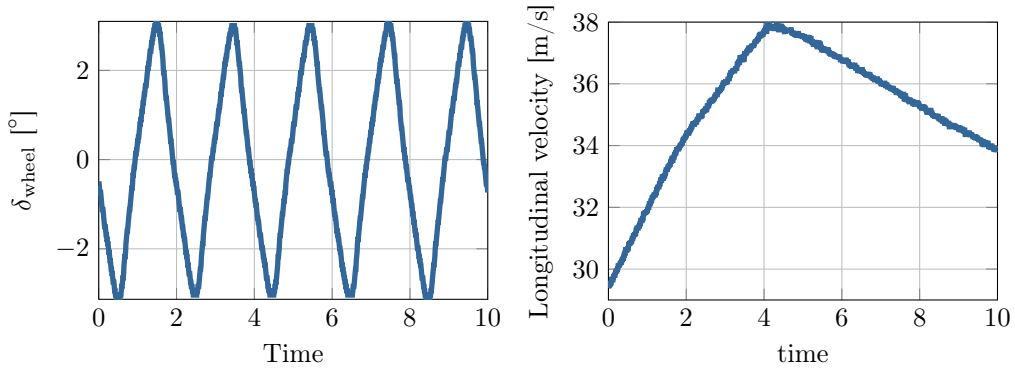

Figure 5.9: (a) Steering profile during measurements. (b) Velocity during measurements.

Figure 5.10 contains the yaw-rate response of the non-linear and the linearized vehicle model on the steering input and the measured yaw-rate response of the actual vehicle. As can be observed, there is almost a similar response of the non-linear and linearized vehicle model and the actual vehicle response. The RMSE between the measured yaw-rate and the yaw-rate calculated by the non-linear model is $0.361°/s$ or a relative error of 0.0394%. Furthermore, the RMSE between the measured yaw-rate and the yaw-rate of the linearized model is $0.357°/s$ or a relative error of 0.039%.

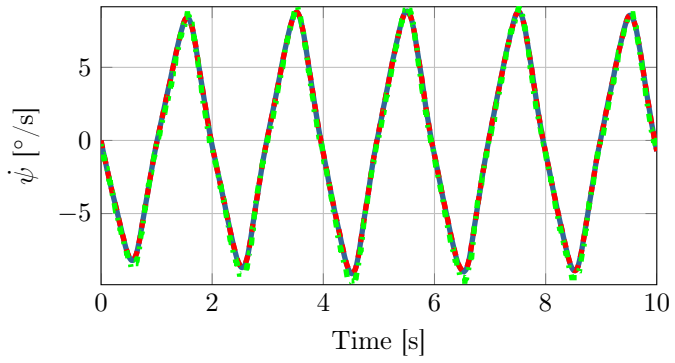

Figure 5.10: Yaw-rate response of the linearized (blue) and non-linear (red) vehicle models and the measured yaw-rate response of the vehicle during the measurements(green).

[1]Test: `3_6`, file: `test_3_06_dat.mat`

However, the measured yaw-rates are significantly higher than the yaw-rates corresponding to linear tyre behavior (Figure 5.4). Therefore, the slip-angles of the non-linear and linearized model are compared to investigate if there is still linear tyre behavior.

Figure 5.11a and Figure 5.11b present the side-slip angles of the front and rear tyres of the non-linear and linearized model. The side-slip angles of rear tyre stay within the interval of $\pm 0.5°$, while the side-slip angles of the front tyre are outside this interval. However, when the RMSE between the side-slip angles of the non-linear and linearized tyre model is only $2.975 \cdot 10^{-5}$. This small error is due the larger interval for which the front tyre still has linear tyre behavior (Figure 4.3a).

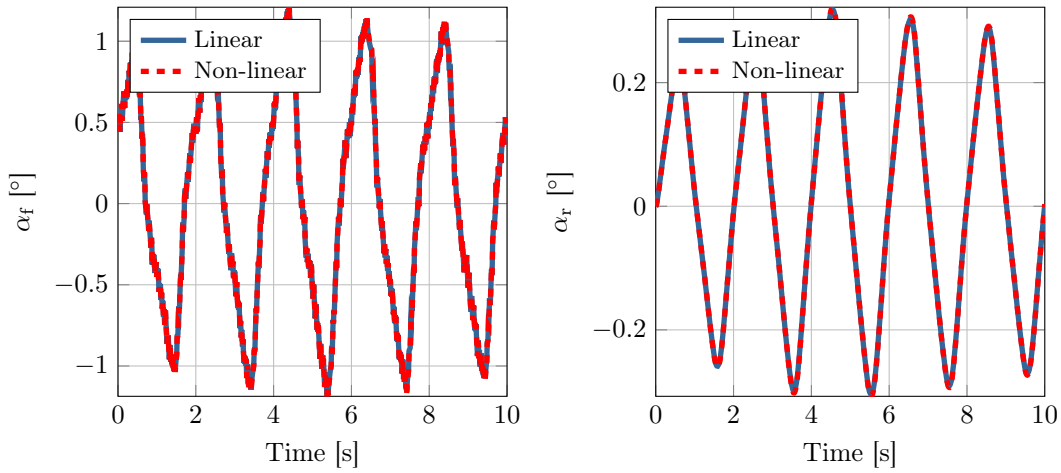

(a) (b)

Figure 5.11: (a) Side-slip angles of the front tyre of the non-linear and linearized model. (b) Side-slip angles of the rear tyre of the non-linear and linearized model.

5.4 Conclusion

In this chapter the dynamic behavior of the non-linear and linearized vehicle model is analyzed. Using simulations it is shown that when the side-slip angles of the tyres stay within $\pm 0.5°$, the non-linear and the linearized vehicle models have the almost the same dynamic response. Furthermore, these conditions also apply for specific maneuvers like lane changes. The final step is the validation of the response of the non-linear and the linearized vehicle model using experimental data. Based on the experimental data gathered at the ATC test track in Aldenhoven, it can be concluded that there is a very small error between the response of the non-linear vehicle model, the linearized vehicle model and the actual vehicle. This means that the linearized vehicle model can be used for controller design.

Chapter 6

Conclusions & Recommendations

The goal of this internship report is to provide an overview of lateral control strategies, present relevant lateral vehicle dynamic models and determine which model is the most suitable for controller design. Two sensing methods and two lateral control strategies are present. When look-down sensing is used the sensor looks straight down onto the road surface, this sensing method was mainly applied in the 90's. The largest drawback of this sensing method is that requires significant investment in the infrastructure and it is also an outdated method. Look-ahead sensing uses sensor(s) that look in front of the vehicle, this method can use either a camera or a radar/LIDAR to look in front of the vehicle. Furthermore, there are two main lateral control strategies, lane following or vehicle following. Lane following can be applied by using look-down sensing or look-ahead sensing, when the vehicle is equipped with a camera. The camera can be used to detected the lane markings on the road, this information can than be further used to determine the position of the vehicle compared to the centerline of the road. Vehicle following can only be applied when look-ahead sensing is used, this can be achieved either by using a camera or a radar/LIDAR. Furthermore, several approaches for determining stability are presented. One approach is to determine what the rearward amplification of the lateral velocity of the cm of the vehicle is. Another method is to determine if a platoon is lateral string stable. Lateral string stability can be determined by assessed l_2-stability for the lateral position error of two preceding vehicle or by calculating the largest singular value of the transfer function. Another possibility is to use the $\mathcal{H}_\infty$-norm for the complementary sensitivity function for the lateral error or combine longitudinal and lateral string stability into mesh-stability and use the $\mathcal{L}_1$-norm of the impulse response to determine stability. However, to the authors knowledge there is no literature available on the synthesis of a lateral controller with guaranteed string stability for an infinite string of vehicles.

Further, three driving scenarios where presented: lane change, merging and vehicle following. Experimental data was gathered on a lane change manoeuver and the occurring yaw rates of the vehicle where analyzed. The manoeuver was conducted with a high frequency to identify the boundaries of the occurring yaw rate, these boundaries for such manoeuvre are $\pm 5 rad/s$.

Furthermore, a non-linear vehicle model with non-linear tyre models and a linearized vehicle model with linearized tyre models is presented. For both models the lateral and yaw dynamics are derived and differences and similarities are demonstrated. Using simulations it is shown that when the side slip angles of the tyres stay within $\pm 0.5^\circ$, the non-linear and the linearized vehicle models have the same dynamic response. Furthermore, these conditions also apply for specific maneuvers like lane changes. The final step is the validation of the response of the non-linear and the linearized vehicle model using experimental data. Based on the measurement data gathered at the ATC test

track in Aldenhoven, it can be concluded that the linear vehicle model with linearized tyre models is able to simulate the lateral and yaw-dynamics accurately. This makes it possible to use linear control theory and linear stability analysis during control synthesis.

6.1 Recommendations and future work

For the development of the lateral controller it is recommended to investigate the possibilities to use WiFi communication to provide extra information on the preceding vehicle. Information communicated via WiFi has often less lag and is more accurate information than the information which is measured by the preceding vehicle. In longitudinal control it has been shown that adding communication leads to smaller inter-vehicle spacings while maintaining string-stable behavior. In longitudinal direction the desired acceleration is communicated, communicating the lateral acceleration of the cm could be a possibility of lateral control. Furthermore, a kinematic vehicle model could be combined with the linearized vehicle model such that it is also possible to perform simulations with low velocities.

Bibliography

Awawdeh, A. M., Espinosa, F., and Mazo, M., (2004). Non-linear trajectory generation and lateral control new algorithms to minimize platoon's oscillations. In *Proceedings of the American Control Conference*, volume 4, pages 3345–3350. IEEE.

Espinosa, F., Awawdeh, A., Mazo, M., Rodriguez, J. M., Bocos, A., and Manzano, M., (2007). Reduction of lateral and longitudinal oscillations of vehicle's platooning by means of decentralized overlapping control. In *46th IEEE Conference on Decision and Control*, pages 690–695. IEEE.

Fancher, P. and Mathew., A. A vehicle dynamics handbook for single-unit and articulated heavy trucks. Technical Report UMTRI-81-21, The University of Michigan Transportation Research Institute, (May 1987).

Hingwe, P. and Tomizuka, M., (1997). Experimental evaluation of a chatter free sliding mode control for lateral control in ahs. In *Proceedings of the American Control Conference*, volume 5, pages 3365–3369. IEEE.

Kang, J., Hindiyeh, R. Y., Moon, S., Gerdes, J. C., and Yi, K., (2008). Design and testing of a controller for autonomous vehicle path tracking using gps/ins sensors. In *Proceedings of the 17th IFAC World Congress, Seoul, Korea*, pages 6–11.

Khatir, M. E. and Davison, E. J., (2005). Decentralized control of a large platoon of vehicles operating on a plane with steering dynamics. In *Proceedings of the American Control Conference*, pages 2159–2165. IEEE.

Khatir, M. E. and Davison, E. J., (2006). A decentralized lateral-longitudinal controller for a platoon of vehicles operating on a plane. In *Proceedings of the American Control Conference*, pages 6–pp. IEEE.

Klančar, G., Matko, D., and Blažič, S., (2011). A control strategy for platoons of differential drive wheeled mobile robot. *Robotics and Autonomous Systems*, 59(2):57–64.

Kosecka, J., Blasi, R., Taylor, C., and Malik, J., (1997). Vision-based lateral control of vehicles. In *IEEE Conference on Intelligent Transportation System*, pages 900–905. IEEE.

Kumarawadu, S. and Lee, T.-T., (2006). Neuroadaptive combined lateral and longitudinal control of highway vehicles using rbf networks. *IEEE Transactions on Intelligent Transportation Systems*, 7(4): 500–512.

Lee, G., Kim, S., Yim, Y., Jung, J., Oh, S., and Kim, B., (1999). Longitudinal and lateral control system development for a platoon of vehicles. In *Proceedings of the IEEE/IEEJ/JSAI International Conference on Intelligent Transportation Systems*, pages 605–610. IEEE.

Lu, G. and Tomizuka, M., (2003). A laser scanning radar based autonomous lateral vehicle following control scheme for automated highways. In *Proceedings of the 2003 American Control Conference*, volume 1, pages 30–35. IEEE.

Lu, G. and Tomizuka, M., (2004). A practical solution to the string stability problem in autonomous vehicle following. In *Proceedings of the American Control Conference*, volume 1, pages 780–785. IEEE.

Luijten, L. Lateral dynamic behaviour of articulated commercial vehicles. Master's thesis, Techinical University Eindhoven, (2010).

Naffin, D. J., Akar, M., and Sukhatme, G. S. Lateral and longitudinal stability for decentralized formation control. In *Distributed Autonomous Robotic Systems 6*, pages 443–452. Springer.

Naus, G. J., Vugts, R. P., Ploeg, J., Molengraft, M. R. J. van de , and Steinbuch, M., (2010). String-stable cacc design and experimental validation: A frequency-domain approach. *IEEE Transactions on Vehicular Technology*, 59(9):4268–4279.

Pacejka, H., (2005). *Tyre and vehicle dynamics*. Elsevier.

Pant, A., Seiler, P., Koo, T. J., and Hedrick, K., (2001). Mesh stability of unmanned aerial vehicle clusters. In *Proceedings of the American Control Conference*, volume 1, pages 62–68. IEEE.

Papadimitriou, I., Lu, G., and Tomizuka, M., (2003). Autonomous lateral following consideration for vehicle platoons. In *Proceedings IEEE/ASME International Conference on Advanced Intelligent Mechatronics*, volume 1, pages 401–406. IEEE.

Papadimitriou, I. and Tomizuka, M., (2004). Lateral control of platoons of vehicles on highways: the autonomous following based approach. *International journal of vehicle design*, 36(1):24–37.

Pauwelussen, J., Anghelache, G., dr. Theodorescu, and Schmeitz, A. Yaw stability of articulated trucks. Leonardo DaVinci, module 10.

Peng, H. and Tomizuka, M., (1990). Vehicle lateral control for highway automation. In *Proceedings of the American Control Conference*, pages 788–794. IEEE.

Peppard, L., (1974). String stability of relative-motion pid vehicle control systems. *IEEE Transactions on Automatic Control*, 19(5):579–581.

Ploeg, J., (2014). *Analysis And Design Of Controllers For Cooperative And Automated Driving*. PhD thesis, Technical University Eindhoven.

Ploeg, J., Scheepers, B. T., Nunen, E. van , Wouw, N. van de , and Nijmeijer, H., (2011). Design and experimental evaluation of cooperative adaptive cruise control. In *14th International IEEE Conference on Intelligent Transportation Systems (ITSC)*, pages 260–265. IEEE.

Ploeg, J., Wouw, N. van de , and Nijmeijer, H., (2014). Lp string stability of cascaded systems: Application to vehicle platooning. *IEEE Transactions on Control Systems Technology*, 22(2):786–793.

Rajamani, R., Zhu, C., and Alexander, L., (2003). Lateral control of a backward driven front-steering vehicle. *Control Engineering Practice*, 11(5):531–540.

Rajamani, R., (2011). *Vehicle dynamics and control*. Springer.

Rajamani, R., Tan, H.-S., Law, B. K., and Zhang, W.-B., (2000). Demonstration of integrated longitudinal and lateral control for the operation of automated vehicles in platoons. *IEEE Transactions on Control Systems Technology*, 8(4):695–708.

Rossetter, E. J. and Gerdes, J. C., (2002). A study of lateral vehicle control under a 'virtual' force framework. In *Proceedings of the International Symposium on Advanced Vehicle Control, Hiroshima, Japan*.

Seiler, P., Pant, A., and Hedrick, J., (2003). A systems interpretation for observations of bird v-formations. *Journal of theoretical biology*, 221(2):279–287.

Shaw, E. and Hedrick, J. K., (2007). Controller design for string stable heterogeneous vehicle strings. In *46th IEEE Conference on Decision and Control*, pages 2868–2875. IEEE.

Shladover, S. E., Desoer, C. A., Hedrick, J. K., Tomizuka, M., Walrand, J., Zhang, W.-B., McMahon, D. H., Peng, H., Sheikholeslam, S., and McKeown, N., (1991). Automated vehicle control developments in the path program. *IEEE Transactions on Vehicular Technology*, 40(1):114–130.

Solyom, S., Idelchi, A., and Salamah, B. B., (2013). Lateral control of vehicle platoons. In *IEEE International Conference on Systems, Man, and Cybernetics (SMC)*, pages 4561–4565. IEEE.

Swaroop, D., (1997). String stability of interconnected systems: An application to platooning in automated highway systems. *California Partners for Advanced Transit and Highways (PATH)*.

Taylor, C. J., Košecká, J., Blasi, R., and Malik, J., (1999). A comparative study of vision-based lateral control strategies for autonomous highway driving. *The International Journal of Robotics Research*, 18(5):442–453.

Wouw, N. van de , (2010). *Lecture Notes, 4J400 - Multibody Dynamics*. TU/e.

Wang, J. and Tomizuka, M., (1999). Robust H_∞ lateral control of heavy-duty vehicles in automated highway system. In *Proceedings of the 1999 American Control Conference*, volume 5, pages 3671–3675. IEEE.

White, R. and Tomizuka, M., (2001). Autonomous following lateral control of heavy vehicles using laser scanning radar. In *Proceedings of the American Control Conference*, volume 3, pages 2333–2338. IEEE.